Stability of the positively charged manganese centre in GaAs heterostructures examined theoretically by the effective mass approximation calculation near the Γ critical point*

Wang Li-Guo(王丽国), Shen Chao(申 超), Zheng Hou-Zhi(郑厚植)†, Zhu Hui(朱 汇), and Zhao Jian-Hua(赵建华)

State Key Laboratory for Superlattices and Microstructures, Institute of Semiconductors, Chinese Academy of Sciences, P.O. Box 912, Beijing 100083, *China*

(Received 4 March 2011; revised manuscript received 10 April 2011)

This paper describes an n–i–p–i–n model heterostructure with a manganese (Mn)-doped p-type base region to check the stability of a positively charged manganese $A^+_{\rm Mn}$ centre with two holes weakly bound by a negatively charged $3d^5$(Mn) core of a local spin $S = 5/2$ in the framework of the effective mass approximation near the Γ critical point ($k \sim 0$). By including the carrier screening effect, the ground state energy and the binding energy of the second hole in the positively charged centre $A^+_{\rm Mn}$ are calculated within a hole concentration range from 1×10^{16} cm^{-3} to 1×10^{17} cm^{-3}, which is achievable by biasing the structure under photo-excitation. For comparison, the ground-state energy of a single hole in the neutral $A^0_{\rm Mn}$ centre is calculated in the same concentration range. It turns out that the binding energy of the second hole in the $A^+_{\rm Mn}$ centre varies from 9.27 meV to 4.57 meV. We propose that the presence of the $A^+_{\rm Mn}$ centre can be examined by measuring the photoluminescence from recombination of electrons in the conduction band with the bound holes in the $A^+_{\rm Mn}$ centre since a high frequency dielectric constant of $\varepsilon_\infty = 10.66$ can be safely adopted in this case. The novel feature of the ability to tune the impurity level of the $A^+_{\rm Mn}$ centre makes it attractive for optically and electrically manipulating local magnetic spins in semiconductors.

Keywords: charged acceptor centre, screening effect, exchange interaction

PACS: 03.65.–w, 61.72.S–, 75.50.Pp **DOI:** 10.1088/1674-1056/20/10/100301

Manganese is one of the most intensively investigated transition-metal impurities[1,2] in GaAs semiconductors. Many experimental techniques, including electron spin resonance,[3] infrared absorption spectroscopy,[4] and magnetization measurements,[5] have proved that the substitution of manganese (Mn) on a Ga site forms an $A^0_{\rm Mn}$ (d^5 + hole)-type acceptor centre in Mn-doped GaAs. This type of centre can be regarded as a rather weakly bound hole around a negatively charged $3d^5$(Mn) core of local spin $S = 5/2$, and shows a ground-state binding energy of 112.4 meV.[6] Recently, it was found that an $A^0_{\rm Mn}$ (d^5 + hole) centre could be electrically manipulated and optically read out in II–VI magnetic quantum dots[7] and a bulk GaAs crystal.[8] In Ref. [8], by detecting photoluminescence (PL) $(e, A^0_{\rm Mn})$ in quantum wells, it was found that optical spin orientation results in a splitting of the Mn–ion spin states, and the polarized Mn spins split the valence-band spin states in return at zero magnetic field. That provides a new scheme of optically addressing and controlling small numbers of magnetic ions in semiconductors without a magnetic field or magnetic materials. To pursue such a goal, one still needs to exploit the important features of Mn centres themselves, such as possible electronic configuration (neutrally or multi-charged), spin coupling schemes,[9] and the influence from quantum confinement and hole concentration,[10] etc. The stability of a positively charged $A^+_{\rm Mn}$ (d^5 + 2 holes) centre in bulk GaAs materials has been theoretically examined in the Hartree approximation, which results in a marginal binding energy for the second bound hole, depending on the choice of crystal dielectric constant.[11] For the infrared absorption spectrum, the calculated binding energy of the second hole tends to vanish, because a static dielectric constant of 12.56 has

*Project partly supported by the National Basic Research Program of China (Grant Nos. 2007CB924904 and 2011CB932901).
†Corresponding author. E-mail: hzzheng@red.semi.ac.cn
© 2011 Chinese Physical Society and IOP Publishing Ltd

to be used. Neutrally and positively charged shallow acceptor centers in p-doped SiGe/Si nanostructures and a multi-charged Mn ion in a p-type InAs quantum disk have also been theoretically studied, and in these systems the valence band mixing and parity change should be explicitly considered due to quantum confinement.[12,13] It turns out that the spins of the two holes are parallel to each other, and then couple anti-parallelly to the 5/2 Mn spin for $A^+_{\rm Mn}$ ($\rm d^5+2$ holes) centers in bulk GaAs,[11] while in quantum dots a singlet two-hole state is preferable, and suppresses its exchange interaction with Mn ions.[13]

In the present work, by designing a model n–i–p–i–n heterostructure with a lightly Mn-doped base layer, one should be able to examine the possible PL from recombination of electrons in the conduction band with the holes in the $A^+_{\rm Mn}$ centre. The hole density is adjustable under photo-excitation by changing the bias on the structure properly. Since we are concerned with a case in which heavy and light holes are well defined at the Γ critical point (where PL occurs) in the absence of quantum confinement, we can re-examine the stability of the $A^+_{\rm Mn}$ centre in clearly defined circumstances, while considering the hole's screening effect in the Thomas–Fermi approximation at the same time.

Our model n–i–p–i–n heterostructure is depicted in Fig. (1a), and the thicknesses of each layers are labeled alongside. The band profiles are schematically shown for zero (solid lines) and negative (dashed lines) biases in Fig. (1b). The doping concentration in the p-type base region is assumed to be $N(M_n) = 1\times10^{17}$ cm^{-3}. Under photo-excitation the hole density in the base layer can be adjusted by changing the bias. The increment of hole concentration under photo-excitation, generated in the 200-nm thick absorption layer and collected in the 10-nm thick Mn-doped region, can be estimated by

$$\Delta p = \frac{P}{\hbar\omega W_2}(1-\mathrm{e}^{-\alpha W_1})\tau,$$

where P is the excitation laser power and α is the GaAs absorption coefficient; $W_1 = 200$ nm and $W_2 = 10$ nm are thicknesses of the absorbing layer and the Mn-doped layer, respectively; τ is the lifetime of photo-carriers in the absorbing region, in which it will be much longer than the ordinary lifetime (on the order of 1 ns) in the flat band case. Here we assume that $P = 0.5$ W/cm^2, $\alpha \approx 2.5\times10^4$ cm^{-1}, and $\tau = 10$ ns $\sim$ 100 ns, Δp can reach the order of 10^{16} cm^{-3} $\sim 10^{17}$ cm^{-3}. As a negative bias is applied, Δp decreases with shortened lifetime τ. In this way one is able to adjust the hole density in the Mn-doped layer in the range from 10^{17} cm^{-3} to 10^{16} cm^{-3}.

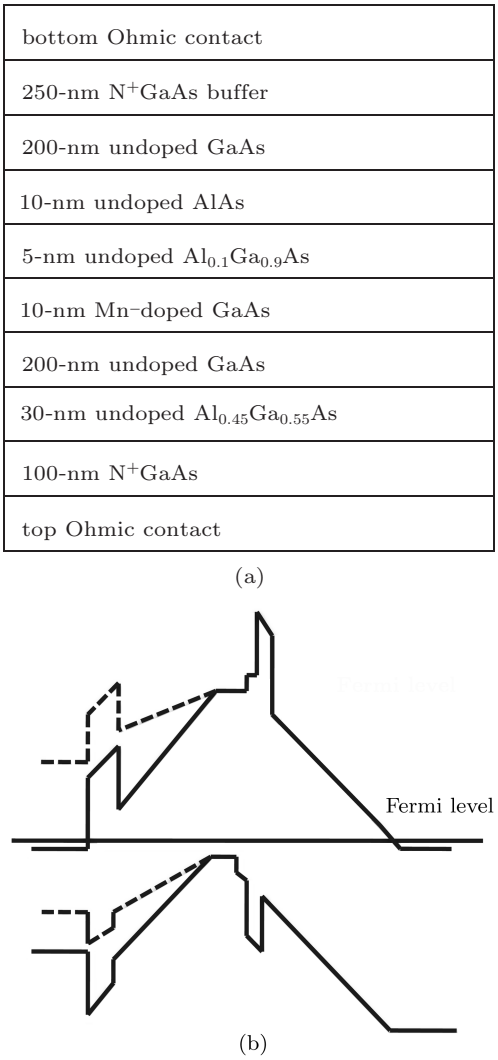


Fig. 1. (a) Layer structure of a model n–i–p–i–n heterostructure with a 10-nm thick, Mn-doped base region, (b) schematic band profiles for zero (solid lines) and negative (dashed lines) biases.

Let us first recall a spherical model of shallow acceptor states in semiconductors, which was proposed as early as 1973[14] recorded in Ref. [15]. It is known that the Luttinger–Kohn Hamiltonian of the valence band in the effective-mass approximation is written in a general form given by

$$\begin{aligned} H_{\rm LK} = &\left(\gamma_1+\frac{5}{2}\gamma_2\right)\frac{p^2}{2m_0} - \frac{\gamma_2}{m_0}\left(p_x^2J_x^2+p_y^2J_y^2+p_z^2J_z^2\right) \\ &- \frac{2\gamma_3}{m_0}[\{p_x,p_y\}\{J_x,J_y\}+\{p_y,p_z\}\{J_y,J_z\} \\ &+\{p_z,p_x\}\{J_z,J_x\}], \end{aligned} \tag{1}$$

where $\{a,b\} = (ab+ba)/2$, m_0 is the free electron mass, γ_1, γ_2, and γ_3 are the Luttinger parameters respectively, $\boldsymbol{p}$ is the hole linear momentum operator

and $\boldsymbol{J}$ is the pseudo-spin angular momentum operator ($J = 3/2$) from the periodic part of the Bloch function of the valence band. The Hamiltonian (1) is valid for a crystal with a diamond structure and in the limit of strong spin–orbit splitting at the Γ point. In the case of a zinc–blende crystal such as GaAs, terms linear in $\boldsymbol{p}$ should be added to Hamiltonian (1). However, as becomes clear later, the contribution to the binding energy from these terms is very small and therefore negligible. Introducing the following second-rank Cartesian tensor operators:[14,15] $P_{ik} = 3p_ip_k - \delta_{ik}p^2$; $J_{ik} = \frac{3}{2}(J_iJ_k + J_kJ_i) - \delta_{ik}J^2$ ($i, k = 1, 2, 3$ represent Cartesian coordinates x, y, z, respectively) and neglecting terms of cubic symmetry, the Luttinger–Kohn Hamiltonian under the spherical approximation can be simplified as

$$H_{\rm LK} = \frac{1}{\hbar^2}p^2 - \frac{1}{9\hbar^2}\mu\left(P^{(2)}\cdot J^{(2)}\right), \tag{2}$$

where the effective Rydberg $R_0 = e^4m_0/2\hbar^2(\varepsilon_r\varepsilon_0)^2\gamma_1$ and effective Bohr radius $a_0 = \hbar^2(\varepsilon_r\varepsilon_0)\gamma_1/e^2m_0$ are taken as the units of energy and length (for GaAs, $R_0 = 15.687$ meV, $a_0 = 43.115$ Å, 1 Å$= 0.1$ nm), ε_0 and ε_r are the vacuum permittivity and the crystal dielectric constant respectively, $\mu = (6\gamma_3 + 4\gamma_2)/5\gamma_1$ has a value of 0.767 for GaAs material. ε_r takes a value of $\varepsilon_\infty = 10.66$ because the PL transition energy is much higher than both LO and TO phonon energies. The dispersion relation corresponding to Hamiltonian (2) reduces to $E_\pm = -(\gamma_1\hbar^2/2m_0)(1 \pm \mu)k^2$ for light (+) and heavy (−) holes, which are really of spherical symmetry, and have different masses for the heavy and light hole bands. Although the $E \sim k$ dispersion, derived under the spherical approximation, is trivial, the use of spherical tensors $P^{(2)}$ and $J^{(2)}$ makes the calculation of neutrally and positively charged Mn acceptors very easy.

Then, the Hamiltonian for $A^0_{\rm Mn}$ ($\rm d^5$ + hole) acceptor is expressed as:

$$H = H_{\rm LK} + V + H_{\rm ex}. \tag{3}$$

Here, $V = (2/r)\,\mathrm{e}^{-r/\lambda} + a\,\mathrm{e}^{-r/b}$ is the Coulomb potential energy. The first term represents the screened Coulomb potential and the second term is the contribution from the central cell correction which is defined by the constants a and b, λ is the Thomas screening length, and written as $\lambda = \hbar(3\pi^2)^{1/3}(\varepsilon_r\varepsilon_0)^{1/2}/(e(m^*)^{1/2}n^{1/6})$, where m^* is the hole effective mass, n is the hole density, $H_{\rm ex} = \varepsilon j\cdot S$ is the simplified p–d exchange interaction between the hole and Mn ion with j and S representing the hole and Mn spin angular momentum. The term $-(1/9\hbar^2)\mu(P^{(2)}\cdot J^{(2)})$ in Hamiltonians (2) and (3) acts as a kind of spin–orbit interaction, so that only the total momentum $\boldsymbol{G} = \boldsymbol{L} + \boldsymbol{J}$ is the constant of motion. Here, $\boldsymbol{L}$ is the orbital angular momentum, $\boldsymbol{J}$ the spin angular momentum from the periodic part of the Bloch wave function at the top of the valence band. This spin–orbit term will couple the different hydrogenic states, but only between the states of $\Delta L = 0, \pm 2$, limited by the selection rule. Due to the spherical symmetry of Hamiltonian $H_{\rm LK}$, one can take the eigenvector in the L–J angular momentum coupling scheme $|L, J, G, G_z\rangle$ as the basis vector to express $1S_{3/2}$ wave function of $A^0_{\rm Mn}$ Hamiltonian as follows:[14,15]

$$\begin{aligned}\phi(1S_{3/2}) =& f_h(r)\,|L = 0, J = 3/2, G = 3/2, G_z\rangle \\ &+ g_h(r)\,|L = 2, J = 3/2, G = 3/2, G_z\rangle\,,\end{aligned} \tag{4}$$

where L, J, and G denote the quantum numbers for the hole's orbital angular momentum, pseudo-spin angular momentum, and total angular momentum, respectively, G_z is the z projection of G and takes the values of $\pm 3/2$ for heavy holes, $f_h(r)$, $g_h(r)$ are the radial trial functions of the form $f_h(r) = \sqrt{2}\alpha^{3/2}\,\mathrm{e}^{-\alpha r}$, $g_h(r) = \sqrt{\frac{2}{3}}\beta^{5/2}r\,\mathrm{e}^{-\beta r}$, which are similar to the trial wave functions used in the hydrogen atom.[16,17] They satisfy a normalized condition of $\int_0^\infty (f_h^2(r) + g_h^2(r))r^2\mathrm{d}r = 1$. The Schrödinger equation for $1\mathrm{S}_{3/2}$ state is derived to be[18]

$$\begin{cases}\left[\dfrac{\mathrm{d}^2}{\mathrm{d}r^2} + \dfrac{2}{r}\dfrac{\mathrm{d}}{\mathrm{d}r} + V(r) - E\right]f_h(r) - \mu\left(\dfrac{\mathrm{d}^2}{\mathrm{d}r^2} + \dfrac{5}{r}\dfrac{\mathrm{d}}{\mathrm{d}r} + \dfrac{3}{r^2}\right)g_h(r) = 0, \\ \left[\dfrac{\mathrm{d}^2}{\mathrm{d}r^2} + \dfrac{2}{r}\dfrac{\mathrm{d}}{\mathrm{d}r} - \dfrac{6}{r^2} + V(r) - E\right]g_h(r) - \mu\left(\dfrac{\mathrm{d}^2}{\mathrm{d}r^2} - \dfrac{1}{r}\dfrac{\mathrm{d}}{\mathrm{d}r}\right)f_h(r) = 0.\end{cases} \tag{5}$$

Eventually, we obtain the minimum energy for the first two terms of the Hamiltonian (3) by conventional variation method (see Appendix A for details), $E(h)_{(H_{\rm LK}+V)} = -85.23$ meV, for a hole concentration of $p = 6\times10^{16}$ cm^{-3} or a screening length of $\lambda = 0.662$.

The energy for the exchange interaction term is determined by $\frac{1}{2}\varepsilon[G(G+1) - \frac{3}{2}(\frac{3}{2}+1) - \frac{5}{2}(\frac{5}{2}+1)]$ with the total angular momentum $G = j+S$ ($G = 1, 2, 3, 4$). For ground state $G = 1$, it has a constant value of -26.25 meV as the exchange coupling parame-

ter $\varepsilon = 5$ meV is adopted from experiments.[15] Finally, the total ground state energy of $A^0_{\rm Mn}$ is equal to $E(h) = -111.48$ meV, which is consistent with previous measurements.

The Hamiltonian for $A^+_{\rm Mn}$ can be expressed as

$$H = H(1) + H(2) + V_{12} = H_{\rm LK}(1) + H_{\rm LK}(2) + V(1) + V(2) + V_{12} + H_{\rm ex}(1) + H_{\rm ex}(2). \quad (6)$$

As in Eq. (3), $H_{\rm LK}(i)$ is still the Luttinger–Kohn Hamiltonian for the i-th hole, $V(i)$ is the Coulomb potential of the Mn core felt by the i-th hole, $H_{\rm ex}(i)$ is the exchange interaction of the i-th hole with Mn spin 5/2 ($i = 1, 2$), V_{12} is the repulsion potential between the two holes.

Before we construct the wave function for $A^+_{\rm Mn}$ centre with two bound holes in it, we point out that the heavy and light holes are well defined at the Γ point ($k = 0$, where PL occurs) in the absence of quantum confinement as in the present case. This is different from Refs. [12] and [13], where the quantum confinement of a quantum disk gives rise to strong valence band mixing and changes the parity of the system, which leads to a unique hole state denoted only by the good quantum numbers of the z component of the total momentum, parity (or pseudo-spin) and orbital quantum number. As a result, the holes behave as if they are indistinguishable.

Since the heavy and light holes are distinguishable in our case, the $A^+_{\rm Mn}$ wave function does not have to be anti-symmetric[12,13] and can be simply written as a product of each individual hole function[17]

$$\begin{aligned}\phi &= |\phi(1)\rangle|\phi(2)\rangle \\ &= [f_{\rm 2h}(r_1)|L=0\rangle_1 + g_{\rm 2h}(r_1)|L=2\rangle_1] \\ &\quad \otimes [f_{\rm 2h}(r_2)|L=0\rangle_2 + g_{\rm 2h}(r_2)|L=2\rangle_2]. \end{aligned} \quad (7)$$

Here, $|L=0\rangle_1 = |L=0,\ J=3/2,\ G=3/2,\ G_z=\pm 3/2\rangle$, $|L=2\rangle_1 = |L=2,\ J=3/2,\ G=3/2,\ G_z=\pm 3/2\rangle$ are for heavy holes; $|L=0\rangle_2 = |L=0,\ J=3/2,\ G=3/2,\ G_z=\pm 1/2\rangle$, $|L=2\rangle_2 = |L=2,\ J=3/2,\ G=3/2,\ G_z=\pm 1/2\rangle$ are for light holes. $f_{\rm 2h}(r)$, $g_{\rm 2h}(r)$ have the same function forms as those used in $A^0_{\rm Mn}$ model. Following the same procedure used for $A^0_{\rm Mn}$, the minimum energy for the first five terms of $A^+_{\rm Mn}$ Hamiltonian (6), turns out to be -95.97 meV (see Appendix B for details).

The exchange energy is calculated to be $E_{\rm ex} = \frac{1}{2}\varepsilon^*[G(G+1) - J(J+1) - \frac{5}{2}(\frac{5}{2}+1)]$. The $E_{\rm ex}$ becomes minimum only when $G = S - J = 5/2 - 2 = 1/2$ and $J = j_1 + j_2 = 3/2 + 1/2 = 2$. This means that the two holes' spins are parallel to each other, and then couple anti-parallelly to the 5/2 Mn spin. We estimate the value of ε^* from ε used in $A^0_{\rm Mn}$ centre. From the expressions

$$\varepsilon = -(1/3)\beta^{p-d}\overline{|f_{\rm h}(0)|^2},$$

and

$$\varepsilon^* = -(1/3)\beta^{p-d}\overline{|f_{\rm 2h}(0)|^2},$$

one knows that these two exchange coupling parameters are both determined by the amplitudes of the hole wave functions at the origin of the Coulomb potentials.[17] We first calculate the theoretical ratio $\overline{f^2_{\rm 2h}(0)}/\overline{f^2_{\rm h}(0)}$, and then obtain $E_{\rm ex} = -7\varepsilon^* = -21.22$ meV by adopting $\varepsilon = 5$ meV. Summing all terms, we finally obtain the ground state energy of -117.19 meV for $A^+_{\rm Mn}$ centre by variation method as $p = 6 \times 10^{16}$ cm^{-3}.

Now it is easy to obtain the binding energy for the second hole. As usual, it is defined as the difference in the total energies between $A^0_{\rm Mn}$ and $A^+_{\rm Mn}$ centres (so-called affinity). Then, the binding energy for the second hole is obtained to be $(-111.48$ meV$) - (-117.19$ meV$) = 5.71$ meV when $p = 6 \times 10^{16}$ cm^{-3}.

Next we study the ground state energies for the neutral $A^0_{\rm Mn}$ centre, positively charged $A^+_{\rm Mn}$ centre, and the binding energy of the second bound hole in the $A^+_{\rm Mn}$ centre, as the hole concentration varies. Table 1 lists the energies of $E(2{\rm h})_{(H_{\rm LK}+V)}$, $E_{\rm REP}$, and $E_{\rm ex}$ under various hole concentrations. One sees that $2E(2{\rm h})_{(H_{\rm LK}+V)} < E({\rm h})_{(H_{\rm LK}+V)} < E(2{\rm h})_{(H_{\rm LK}+V)}$ over the concentration range studied here (note their negative sign). The single hole energy $E(2{\rm h})_{(H_{\rm LK}+V)}$ in $A^+_{\rm Mn}$ centre is less negative than that in the $A^0_{\rm Mn}$ centre because of its deviation from the Coulomb potential centre caused by the repulsion between the two holes. The deviation of each bound hole from the Coulomb potential centre also reduces its exchange interaction with the Mn 5/2 spin in the 3d shell, and leads to a less negative exchange energy. But the total energy of the two holes is more negative than the single hole energy in $A^0_{\rm Mn}$ centre, and decreases with increasing hole concentration due to enhanced screening. Also the positive Coulomb repulsion energy between the two holes is reduced for the same reason. The calculated binding energy for the second hole in the $A^+_{\rm Mn}$ centre is given in Table 2 for different hole concentrations within a range from 1×10^{17} cm^{-3} to 1×10^{16} cm^{-3}. The binding energy of the second hole increases from 4.57 meV up to 7.29 meV. Up to now one may be convinced that $A^+_{\rm Mn}$ centre should be stable in a rather wide concentration of holes, and can be detected by PL in our model heterostructure.

Table 1. The minimum energies of a single hole in the Coulomb potentials of the $A^0_{\rm Mn}$ and $A^+_{\rm Mn}$ centres respectively, and the minimum energies of exchange energies and Coulomb repulsion energies in the $A^+_{\rm Mn}$ centre calculated at various hole concentrations.

$p/{\rm cm}^{-3}$	λ	$A^0_{\rm Mn}$		$A^+_{\rm Mn}$		
		$E({\rm h})_{(H_{\rm LK}+V)}$/meV	$E_{\rm ex}$/meV	$E(2{\rm h})_{(H_{\rm LK}+V)}$/meV	$E_{\rm REP}$/meV	$E_{\rm ex}$/meV
1×10^{17}	0.607	−84.03	−26.25	−52.97	12.04	−20.95
8×10^{16}	0.631	−84.63	−26.25	−53.52	12.07	−21.08
6×10^{16}	0.662	−85.23	−26.25	−54.04	12.11	−21.22
4×10^{16}	0.707	−85.80	−26.25	−54.79	12.17	−21.48
2×10^{16}	0.794	−87.22	−26.25	−55.95	12.20	−21.73
1×10^{16}	0.892	−88.55	−26.25	−57.15	12.24	−22.01

Table 2. Ground state energies of $A^0_{\rm Mn}$, $A^+_{\rm Mn}$ centres and the second hole's binding energy $E^{(2)}_{\rm I}$ calculated at different hole densities. The superscript $*$ indicates that each number in summation inside the bracket gives the minimum energies, $E({\rm h})_{(H_{\rm LK}+V)}$ and $E_{\rm EX}$, respectively in the case of $A^0_{\rm Mn}$ centre, and $2E(2{\rm h})_{(H_{\rm LK}+V)}$, $E_{\rm REP}$, and $E_{\rm EX}$, respectively in the case of $A^+_{\rm Mn}$ centre.

p /cm^{-3}	λ	$E(A^0_{\rm Mn})$/meV	$E(A^+_{\rm Mn})$/meV	$E^{(2)}_{\rm I}$/meV
1×10^{17}	0.607	$-110.28(-84.03-26.25)^*$	$-114.85(-105.94+12.04-20.95)^*$	4.57
8×10^{16}	0.631	$-110.88(-84.63-26.25)^*$	$-116.05(-107.04+12.07-21.08)^*$	5.17
6×10^{16}	0.662	$-111.48(-85.23-26.25)^*$	$-117.19(-108.08+12.11-21.22)^*$	5.71
4×10^{16}	0.707	$-112.05(-85.80-26.25)^*$	$-118.89(-109.58+12.17-21.48)^*$	6.84
2×10^{16}	0.794	$-113.47(-87.22-26.25)^*$	$-121.43(-111.90+12.20-21.73)^*$	7.96
1×10^{16}	0.892	$-114.80(-88.55-26.25)^*$	$-124.07(-114.30+12.24-22.01)^*$	9.27

In conclusion, the stability of a positively charged manganese (Mn) $A^+_{\rm Mn}$ centre with two holes weakly bound by negatively a charged $3{\rm d}^5$(Mn) core of a local spin $S=5/2$ has been theoretically examined in the n–i–p–i–n model heterostructure with a manganese-doped p-type base region using the effective mass approximation calculation near the Γ critical point ($k\sim0$). It is suggested that the presence of the $A^+_{\rm Mn}$ centre can be examined by measuring the photoluminescence from recombination of electrons in the conduction band with the bound holes in the $A^+_{\rm Mn}$ centre in such a structure, since a high frequency dielectric constant of $\varepsilon_\infty=10.66$ can be safely adopted in PL measurements. The binding energy of the second hole in the $A^+_{\rm Mn}$ centre varies from 9.27 meV to 4.57 meV within a hole concentration range from 1×10^{16} cm^{-3} to 1×10^{17} cm^{-3}. The latter is achievable by biasing the n–i–p–i–n model heterostructure under photo-excitation. The novel feature of the ability to tune the impurity level of the $A^+_{\rm Mn}$ centre makes it attractive for optically and electrically manipulating local magnetic spins in semiconductors.

Appendix A: Single hole in the $A^0_{\rm Mn}$ centre

Since the $1S_{3/2}$ wave function of $A^0_{\rm Mn}$ Hamiltonian is expressed as Eq. (4) as given previously, (where $L=4$, $L=6$, etc. states are neglected for simplicity, its Schrödinger equation is of the form

$$\begin{bmatrix} A & B \\ C & D \end{bmatrix}\begin{bmatrix} f \\ g \end{bmatrix} = E\begin{bmatrix} f \\ g \end{bmatrix}, \tag{A1}$$

where

$$\begin{cases} A=\dfrac{{\rm d}^2}{{\rm d}r^2}+\dfrac{2}{r}\dfrac{\rm d}{{\rm d}r}+V(r), \\ B=-\mu(\dfrac{{\rm d}^2}{{\rm d}r^2}+\dfrac{5}{r}\dfrac{\rm d}{{\rm d}r}+\dfrac{3}{r^2}), \\ C=-\mu(\dfrac{{\rm d}^2}{{\rm d}r^2}-\dfrac{1}{r}\dfrac{\rm d}{{\rm d}r}), \\ D=\dfrac{{\rm d}^2}{{\rm d}r^2}+\dfrac{2}{r}\dfrac{\rm d}{{\rm d}r}-\dfrac{6}{r^2}+V(r). \end{cases} \tag{A2}$$

From the relations

$$\langle L',J,F|\frac{1}{\hbar^2}p^2+V(r)|L,J,F\rangle = \left[-\frac{1}{r^2}\frac{\rm d}{{\rm d}r}\Big(r^2\frac{\rm d}{{\rm d}r}\Big)+\frac{L(L+1)}{r^2}+V(r)\right]\delta_{L,L'}, \tag{A3}$$

$$\langle L',J,F|(P^{(2)}\cdot J^{(2)})|L,J,F\rangle = (-1)^{L+J+F}\begin{Bmatrix} F,J,L' \\ 2,L,J \end{Bmatrix}\langle J|J^{(2)}|J\rangle\langle L'|P^{(2)}|L\rangle, \tag{A4}$$

where $\left\{ \begin{matrix} F, J, L' \\ 2, L, J \end{matrix} \right\}$ is the 6-j symbol, it follows that the Schrödinger equation for $1S_{3/2}$ states of $A^0_{\rm Mn}$ Hamiltonian can be derived to be Eq. (5).

The expectation value for the first two terms of the Hamiltonian (3) is calculated as

$$\begin{aligned} E(\mathrm{h})_{(H_{\rm LK}+V)} &= \int_0^\infty fAfr^2\mathrm{d}r + \int_0^\infty fBgr^2\mathrm{d}r + \int_0^\infty gCfr^2\mathrm{d}r + \int_0^\infty gDgr^2\mathrm{d}r \\ &= \alpha^2\Big[-0.5 + \frac{4\alpha}{(1.667+2\alpha)^2} + \frac{152\alpha}{(2+2\alpha)^3}\Big] - 1.1665\beta^2 - \frac{3.542(4\alpha+\beta)}{(\alpha+\beta)^4} \\ &\quad + \beta^5\Big[\frac{8}{(1.667+2\beta)^4} + \frac{608}{(2+2\beta)^5}\Big]. \end{aligned} \tag{A5}$$

To find the minimum of $E(\mathrm{h})_{(H_{\rm LK}+V)}$ numerically, we plot a series of iso-energy contours at different values of $E(\mathrm{h})_{(H_{\rm LK}+V)}$ in the (α, β) plane, until we obtain satisfactory accuracy in the values of α and β, as shown in Fig. A1.

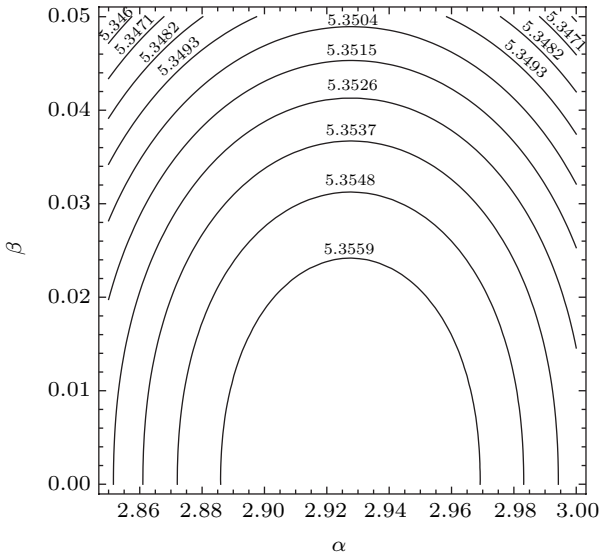


Fig. A1. Iso-energy contour plot of $E(\mathrm{h})_{(H_{\rm LK}+V)}$ for the $A^0_{\rm Mn}$ state plotted in the (α, β) parameter plane when $p = 1\times10^{17}$ cm^{-3}.

Appendix B: Double holes in the $A^+_{\rm Mn}$ centre

As explained in the text, the $A^+_{\rm Mn}$ wave function does not have to be anti-symmetric and can be simply written as a product of each individual hole function as Eq. (7) given before. As stated previously,

$$\begin{aligned} |L=0\rangle_1 &= |L=0, J=3/2, G=3/2, G_z=\pm3/2\rangle, \\ |L=2\rangle_1 &= |L=2, J=3/2, G=3/2, G_z=\pm3/2\rangle \end{aligned}$$

are for heavy holes;

$$\begin{aligned} |L=0\rangle_2 &= |L=0, J=3/2, G=3/2, G_z=\pm1/2\rangle, \\ |L=2\rangle_2 &= |L=2, J=3/2, G=3/2, G_z=\pm1/2\rangle \end{aligned}$$

are for light holes. $f_{2\rm h}(r)$ and $g_{2\rm h}(r)$ have the same function forms as used in $A^0_{\rm Mn}$ model. The expectation value of the first four terms in Hamiltonian (6) can be calculated in the same way as in Appendix A, and equals

$$\begin{aligned} &E(2\mathrm{h})_{(H_{\rm LK}+V)} \\ &\quad = \alpha^2\Big[-0.5 + \frac{4\alpha}{(1.667+2\alpha)^2} + \frac{112\alpha}{(2+2\alpha)^3}\Big] \\ &\qquad - 1.1665\beta^2 - \frac{3.542(\alpha\beta)^{5/2}(4\alpha+\beta)}{(\alpha+\beta)^4} \\ &\qquad + \beta^5\Big[\frac{8}{(1.667+2\beta)^4} + \frac{448}{(2+2\beta)^5}\Big]. \end{aligned} \tag{B1}$$

The derivation of the expectation value $E_{\rm REP}$ of the Coulomb repulsion term

$$\begin{aligned} \langle\phi|\frac{1}{|\boldsymbol{r}_1-\boldsymbol{r}_2|}|\phi\rangle &= ({}_1\langle L=0|\,{}_2\langle L=0|\, f(r_1)f(r_1) \\ &\quad + {}_1\langle L=0|\,{}_2\langle L=2|\, f(r_1)g(r_2) \\ &\quad + {}_2\langle L=0|\,{}_1\langle L=2|\, f(r_2)g(r_1) \\ &\quad + {}_1\langle L=2|\,{}_2\langle L=2|\, g(r_1)g(r_2))\frac{1}{r_{12}}\,|\phi\rangle \end{aligned} \tag{B2}$$

is very tedious, and contains four terms. With the help of the following relations:

$$\frac{1}{r_{12}} = \begin{cases} \displaystyle\sum_{l=0}^{\infty}\sum_{m=-l}^{l}\frac{4\pi}{2l+1}\frac{r_1^l}{r_2^{l+1}}\mathrm{Y}^*_{lm}(\theta_1,\varphi_1)\mathrm{Y}^*_{lm}(\theta_2,\varphi_2);\ r_1<r_2, \\ \displaystyle\sum_{l=0}^{\infty}\sum_{m=-l}^{l}\frac{4\pi}{2l+1}\frac{r_2^l}{r_1^{l+1}}\mathrm{Y}^*_{lm}(\theta_1,\varphi_1)\mathrm{Y}^*_{lm}(\theta_2,\varphi_2);\ r_2<r_1, \end{cases} \tag{B3}$$

the above integrations can be evaluated as follows. For the first term, one has

$$\int_0^\infty f^2(r_1)f^2(r_2)\frac{1}{r_{12}}\frac{1}{16\pi^2}\,\mathrm{d}\boldsymbol{r}_1\,\mathrm{d}\boldsymbol{r}_2 = \frac{4\alpha^6}{16\pi^2}16\pi^2\int_0^\infty r_2^2\,\mathrm{d}r_2\,\mathrm{e}^{-2\alpha r_2}\left\{\frac{1}{r_2^2}\int_0^{r_2} r_1^2\,\mathrm{e}^{-2\alpha r_1}\,\mathrm{d}r_1 + \int_{r_2}^\infty r_1\,\mathrm{e}^{-2\alpha r_1}\,\mathrm{d}r_1\right\}$$
$$= \frac{5}{32}\alpha. \tag{B4}$$

The second term is simplified as

$$\int_0^\infty f^2(r_1)\,g^2(r_2)\mathrm{Y}_{00}^*(\theta_1,\varphi_1)\mathrm{Y}_{20}^*(\theta_2,\varphi_2)\mathrm{Y}_{00}(\theta_1,\varphi_1)\mathrm{Y}_{20}(\theta_2,\varphi_2)\frac{1}{r_{12}}\,\mathrm{d}\boldsymbol{r}_1\,\mathrm{d}\boldsymbol{r}_2$$
$$= \int_0^\infty \mathrm{d}r_2\int_0^{r_2}\mathrm{d}r_1 r_1^2 r_2 f^2(r_1)g^2(r_2)\int \mathrm{Y}_{00}^*(\theta_1,\varphi_1)\mathrm{Y}_{00}(\theta_1,\varphi_1)\,\mathrm{d}\Omega_1\int \mathrm{Y}_{20}(\theta_2,\varphi_2)\mathrm{Y}_{20}(\theta_2,\varphi_2)\,\mathrm{d}\Omega_2$$
$$+\int_0^\infty \mathrm{d}r_2\int_{r_2}^\infty\mathrm{d}r_1 r_1 r_2^2 f^2(r_1)g^2(r_2)\int \mathrm{Y}_{00}^*(\theta_1,\varphi_1)\mathrm{Y}_{00}(\theta_1,\varphi_1)\,\mathrm{d}\Omega_1\int \mathrm{Y}_{20}^*(\theta_2,\varphi_2)\mathrm{Y}_20(\theta_2,\varphi_2)\,\mathrm{d}\Omega_2$$
$$= 2\alpha^3\frac{2}{3}\beta^5\left\{\int_0^\infty \mathrm{d}r_2\int_0^{r_2}\mathrm{d}r_1 r_1^2 r_2^3\,\mathrm{e}^{-2\alpha r_1}\,\mathrm{e}^{-2\beta r_2} + \int_0^\infty \mathrm{d}r_2\int_{r_2}^\infty \mathrm{d}r_1 r_1 r_2^4\,\mathrm{e}^{-2\alpha r_1}\,\mathrm{e}^{-2\beta r_2}\right\}. \tag{B5}$$

The last expression of (Eq. (B5)) can be easily evaluated by using the software Mathematica.

The third term

$$\int_0^\infty f^2(r_2)g^2(r_1)\mathrm{Y}_{00}^*(\theta_2,\varphi_2)\mathrm{Y}_{20}^*(\theta_1,\varphi_1)\mathrm{Y}_{00}(\theta_2,\varphi_2)\mathrm{Y}_{20}(\theta_1,\varphi_1)\frac{1}{r_{12}}\,\mathrm{d}\boldsymbol{r}_1\,\mathrm{d}\boldsymbol{r}_2 \tag{B6}$$

is indeed equal to the second term as seen by exchanging r_1 and r_2.

The last term is evaluated as

$$\int_0^\infty g^2(r_1)g^2(r_2)\mathrm{Y}_{20}^*(\theta_1,\varphi_1)\mathrm{Y}_{20}^*(\theta_2,\varphi_2)\mathrm{Y}_{20}(\theta_1,\varphi_1)\mathrm{Y}_{20}(\theta_2,\varphi_2)\frac{1}{r_{12}}\,\mathrm{d}\boldsymbol{r}_1\,\mathrm{d}\boldsymbol{r}_2$$
$$= 4\pi\frac{4}{9}\beta^{10}\left\{\sum_{l=0}^\infty\frac{1}{2l+1}\left[\int_0^\infty\mathrm{d}r_2\int_0^{r_2}\mathrm{d}r_1\frac{r_1^{l+4}r_2^4}{r_2^{l+1}}\,\mathrm{e}^{-2\beta(r_1+r_2)}\right]\left(\int|\mathrm{Y}_{20}|^2\mathrm{Y}_{l0}\,\mathrm{d}\Omega\right)^2\right.$$
$$\left.+\sum_{l=0}^\infty\frac{1}{2l+1}\left[\int_0^\infty\mathrm{d}r_2\int_{r_2}^\infty\mathrm{d}r_1\frac{r_1^4r_2^{l+4}}{r_1^{l+1}}\,\mathrm{e}^{-2\beta(r_1+r_2)}\right]\left(\int|\mathrm{Y}_{20}|^2\mathrm{Y}_{l0}\,\mathrm{d}\Omega\right)\right\}. \tag{B7}$$

This has non-zero contributions only for $L = 0, 2, 4$, and can also be evaluated by the software Mathematical. Finally, one obtains the expectation value of the Coulomb repulsion energy,

$$E_{\mathrm{REP}} = 0.15625\alpha + 0.0726752\alpha^3\beta^5 + 10.1569\beta^{10}$$
$$+\frac{4\alpha^3\beta^5}{(\alpha+\beta)^7}+\frac{283.277\alpha^{3/2}\beta^{15/2}}{(\alpha+\beta)(\alpha+3\beta)^7}$$
$$+\frac{11.8032\alpha^{3/2}\beta^{15/2}(\alpha+15\beta)}{\beta^2(\alpha+3\beta)^7}. \tag{B8}$$

Following the same procedure as used for A^0_{Mn}, the minimum energy for the first five terms of the A^+_{Mn} Hamiltonian (6) turns out to be

$$2E(2\mathrm{h})_{(H_{\mathrm{LK}}+V)} + E_{\mathrm{REP}} = -95.97\ \mathrm{meV}.$$

The corresponding iso-energy contour in α–β plane is plotted in Fig. A2.

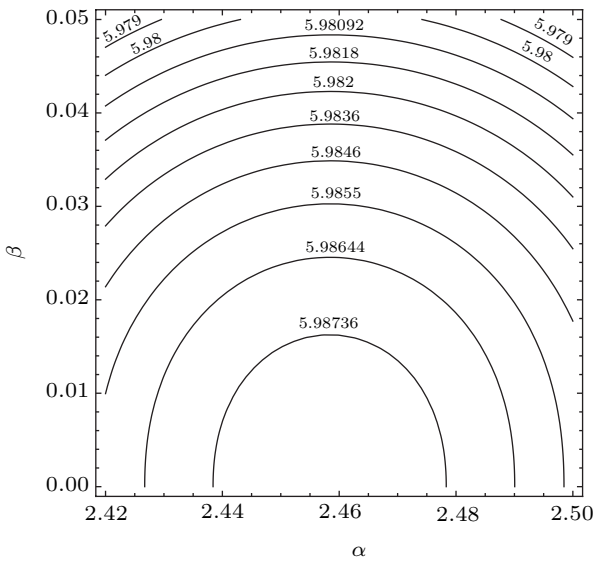


Fig. A2. Iso-energy contour plot of $2E(2\mathrm{h})_{(H_{\mathrm{LK}}+V)} + E_{\mathrm{REP}}$ for A^+_{Mn} state, plotted in (α, β) parameter plane when $p = 1\times10^{17}$ cm^{-3}.

References

[1] Liu X C, Chen Z Z, Shi E W, Liao D Q and Zhou K J 2011 *Chin. Phys.* B **20** 037501

[2] Weng Z Z, Zhang J M, Huang Z G and Lin W X 2011 *Chin. Phys.* B **20** 027103

[3] Schneider J, Kaufmann U, Wilkening W, Baeumler M and Köhl F 1987 *Phys. Rev. Lett.* **59** 240

[4] Tarhan E, Miotkowski I, Rodriguez S and Ramdas A K 2003 *Phys. Rev.* B **67** 195202

[5] Frey T, Maier M, Schneider J and Gehrke M 1988 *J. Phys.* C **21** 5539

[6] Jungwirth T, Sinova J, Mašek J and MacDonald A H 2006 *Rev. Mod. Phys.* **78** 809

[7] Besombes L, Leger Y, Maingault L, Ferrand D, Mariette H and Cigert J 2004 *Phys. Rev. Lett.* **93** 207403

[8] Myers R C, Mikkelsen M H, Tang J M, Gossard A C, Flatt'e M E and Awschalom D D 2008 *Nat. Mater.* **7** 203

[9] Gao Q, Lou X Y, Qi Y and Shan W G 2011 *Acta Phys. Sin.* **60** 036401 (in Chinese)

[10] Su P, Gong M, Ma Y, Gao B, Shi R Y, Chen C, Shi T F, Cao X C, Meng X H and Luo D S 2011 *Acta Phys. Sin.* **60** 027105 (in Chinese)

[11] Bhattacharjee A K and Benoit à la Guillaume C 2000 *Solid State Commun.* **113** 17

[12] Rego L G C, Brum J A and Hawrylak P 1998 *Physica* E **2** 785

[13] Climente J I, Korkusiñski M, Hawrylak P and Planelles J 2005 *Phys. Rev.* B **71** 125321

[14] Baldereschi A and Lipari N O 1973 *Phys. Rev.* B **8** 2697

[15] See Subsubsection 4.2.4 (pp. 164–170) in Yu P Y and Cardona M 1999 *Fundamentals of Semiconductors Physics and Materials Properties* 2nd edn. (Berlin, Heidelberg: Springer-Verlag)

[16] Lipari N O and Baldereschi A 1970 *Phys. Rev. Lett.* **25** 1660

[17] Mendelson K S and James H M 1964 *J. Phys. Chem. Solids* **25** 729

[18] Chutia S and Bhattacharjee A K 2008 *Phys. Rev.* B **78** 195311